https://doi.org/10.15407/ufm.25.04.736

P.E. MARKOVSKY[1,*], S.V. AKHONIN[2,], V.O. BEREZOS[2,***], O.O. STASIUK[1,****], V.I. BONDARCHUK[1], D.V. ORYSHYCH[1], Ye.I. LIPCHANCHUK[2], and O.V. ZATSARNA[1]**

[1] G.V. Kurdyumov Institute for Metal Physics of the N.A.S. of Ukraine, 36, Academician Vernadsky Blvd., UA-03142 Kyiv, Ukraine

[2] E.O. Paton Electric Welding Institute of the N.A.S. of Ukraine, 11, Kazymyr Malevych Str., UA-03150 Kyiv, Ukraine

* pmark@imp.kiev.ua, p_markovsky@yahoo.com, ** akhonin.sv@gmail.com, *** ewi.nasu@gmail.com, **** olek.stasiuk@gmail.com

LAYERED TITANIUM-BASED MATERIALS MANUFACTURED WITH CAST AND WROUGHT: PRODUCTION, COMPOSITION, MICROSTRUCTURE, AND MECHANICAL PROPERTIES

The features of formation of the structure, composition and certain mechanical properties of layered materials based on titanium and its alloys during melting by the electron-beam cold-hearth melting technique are considered. The influence of composition in two-layer structures Ti64 (Ti–6Al–4V)/LCB (low-cost beta Ti–1.5Al–6.8Mo–4.5Fe) and Ti64/Ti5553 (Ti–5Al–5V–5Mo–3Cr), as well as 4-layer Ti5553/Ti64/c.p.Ti (commercial purity titanium)/Ti64 is studied. The processes of formation of transition layers at the boundaries between alloys after both the smelting and the subsequent deformation by rolling, as well as after heat treatments, are studied. A relationship is established between the composition and the formed microstructure, on the one hand, and hardness, strength, ductility, and fracture under 3-point bending, on the other hand. A comparison of the titanium-layered materials produced by this method with the results provided by other technological approaches is carried out, and the advantages of the proposed technology are shown.

Keywords: titanium alloys, layered metal materials, electron-beam cold-hearth melting, microstructure, hardness, strength, ductility.

Citation: P.E. Markovsky, S.V. Akhonin, V.O. Berezos, O.O. Stasiuk, V.I. Bondarchuk, D.V. Oryshych, Ye.I. Lipchanchuk, and O.V. Zatsarna, Layered Titanium-Based Materials Manufactured with Cast and Wrought: Production, Composition, Microstructure, and Mechanical Properties, *Progress in Physics of Metals*, **25**, No. 4: 736–764 (2024)

© Publisher PH "Akademperiodyka" of the NAS of Ukraine, 2024. This is an open access article under the CC BY-ND license (https://creativecommons.org/licenses/by-nd/4.0)

1. Introduction

Titanium alloys are important structural materials possessing many combinations of unique physical and mechanical properties that other metallic materials cannot provide [1–3]. However, having a unique combination of specific strength, fatigue strength, chemical resistance and non-magnetic, they have certain disadvantages, for example, relatively low wear resistance. These disadvantages can be eliminated, and the advantageous properties can be significantly enhanced through the formation of multilayer structures based on titanium [4–7]. These laminated (multilayered) structures of titanium alloys and materials on the base of titanium are promising structural materials for many applications. Their promise is due to the possibility of obtaining a unique combination of properties, when some layers, for example, surface layers, provide high strength, fatigue or wear resistance, while others have high ductility [4–9]. Such layered structures can be formed using a variety of technological approaches. For instance, in the case of conventional alloys of homogeneous composition, a layered/gradient microstructure can be formed by means of surface (local) heat treatment [10–14]. In a certain sense, similar materials include those obtained by surface chemical-thermal treatment [15, 16], or by applying coatings using various methods [17–19]. To form thicker layers, it is more technologically advanced to use powder metallurgy methods [9, 20], or the recently actively developing methods of additive technologies [6, 21]. The work [22] also can be mentioned, in which a two-layer Ti64/c.p.Ti material was produced by explosion welding, and its dynamic behaviour was studied.

However, it was shown earlier that the most cost-effective and simple way to produce titanium alloys on an industrial scale is a single electron-beam cold-hearth melting (EBCHM), followed by direct rolling [23–25]. Moreover, this approach makes it possible to produce not only the common widely used Ti–6Al–4V (wt.%) alloy, but also other, more complex alloys with achieving high mechanical and special service properties [26, 27]. In a certain sense, something similar is the surfacing of titanium materials with an electron beam using Ti–6Al–4V wire [27]. However, this process has relatively lower productivity and higher cost of final products as compared with conventional EBCHM. The superiority of the conventional EBCHM method consists in both its higher productivity and the possibility of using either pure metals or master alloys as starting materials whose cost is much lower as compared to wires, and especially to pre-alloyed titanium alloy powders used in several 3*D*-printing approaches [28–30]. Therefore, in this work, the possibility of producing multilayer titanium alloys by alternate surfacing of titanium alloys of different chemical compositions produced by melting the original pure metals/alloys with an electron beam was considered for the first time. The main idea was to combine/alternate

layers of alloys that have different strengths and ductility, which, as was shown earlier, should significantly increase some special properties of such a layered material [4–9].

2. Features of Material Production and Testing Procedures

The multilayer ingot was produced using the electron beam melting technique by layer-by-layer horizontal surfacing of different grades of alloys in a stationary copper mould on the UE-208M electron-beam unit [30–33]. The features of the process were as follows (see Fig. 1, *a*). A composite blank of (3) appropriate grades of alloys was loaded into the stationary box. The composite billet consisted of the materials required to form the layers in the ingot (Alloys 1–4). The difference in the structure of the final ingot (2- or 4-layered one) is shown in Figs. 1, *b* and *c*. The positions and weights of the layers corresponded to their deposition order and thickness in the melted multilayer ingot. The deposition was carried out in a stationary horizontal copper water-cooled mould (*1* in Fig. 1, *a* and general view in Fig. 2).

The unit was evacuated to the working vacuum in the melting chamber $(6.6–12)\cdot10^{-2}$ Pa. Under the electron beams of two guns (*2*), the component charge billet (*3*), which was fed horizontally, melted and flowed to the bottom of the copper mould (*1*). The liquid metal in the mould was uniformly heated over the entire plane by electron beams (2). The metal melted into the copper mould and solidified from the bottom up. At the end of the melting of the first component of the workpiece, the power of electron beam heating of the surface of the melt was reduced until its complete solidification. After that, the initial metal of the second component was melted in a copper crucible, the melt (*5*) of which was spread evenly over the entire surface of the previous layer (*4*) which had already solidified.

During the formation of a liquid layer of the metal of the second component, the power of electron beams was increased to values that provided the metal mirror with liquid over the entire surface of the copper mould. After the deposition of the second component, the power of the electron beam was gradually reduced in order to prevent the formation of shrinkage voids and looseness in the upper part of the multilayer ingot until complete solidification of melt of the second component. Thus, the process was repeated until the required number of metal layers was formed in a multi-layer ingot (Fig. 3). Depending on the change in the melting point of the metal in the deposited layers, the power of electron beams was also changed accordingly. Specially selected technological modes of the process ensured a reliable connection of the metal layers after solidification over the entire deposited surface and prevented melting of the previous layer by the next one. It should be noted that increasing or decreasing the heat-

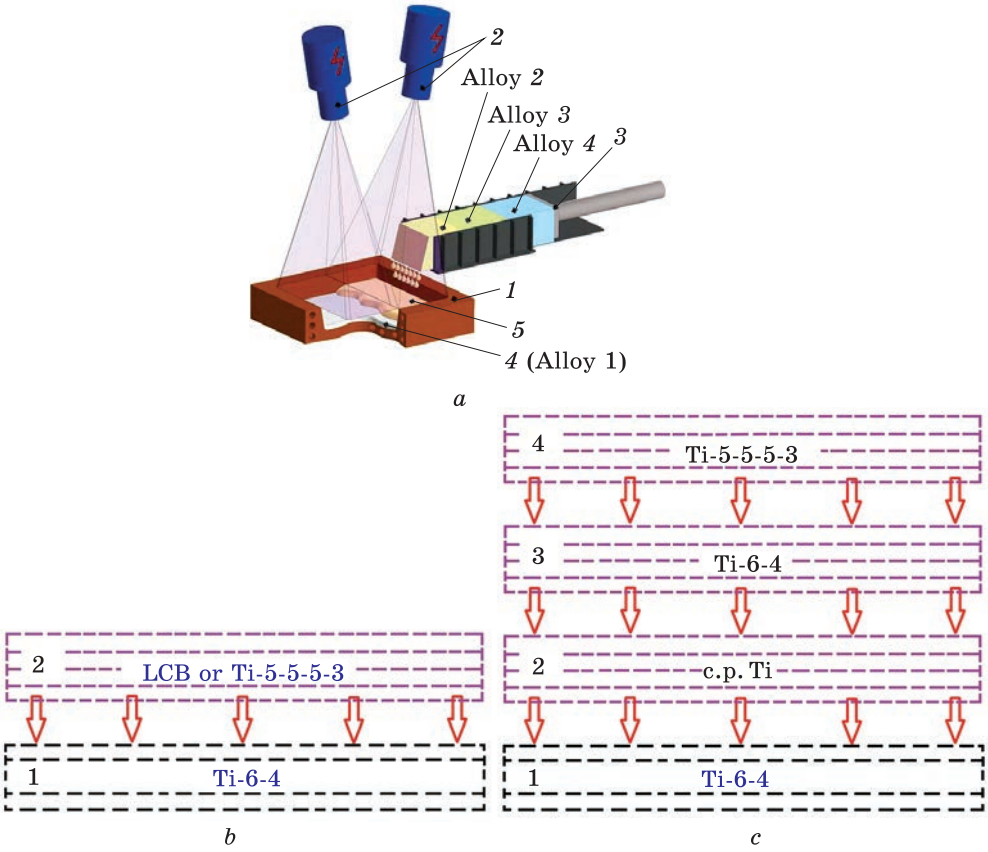

Fig. 1. Schemes of multilayer ingot manufacturing with electron-beam melting technique (*a*) and design of cast billets consisted of two alloys (*b*) and three alloys in four layers (*c*)

Fig. 2. Copper water-cooled mould

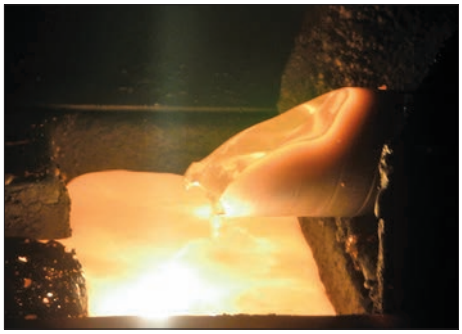

Fig. 3. Process of melting a layer of multilayered ingot

ing power of the layers made it possible to provide any thickness of the transition zone between individual layers with a gradual change in chemical composition. This technology of electron beam melting makes it pos-

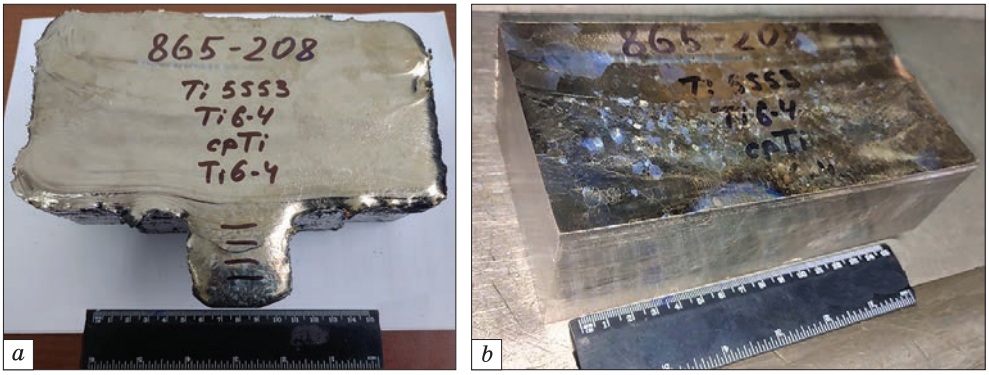

Fig. 4. General view of cast (*a*) and machined (*b*) cast billets of 4-layered Ti64/c.p.Ti/Ti64/Ti5553 material

sible to produce multilayer ingots with any number and width of layers (Fig. 4, *a*). After producing the multilayer ingot, its side faces were mechanically processed to eliminate defects of foundry origin (Fig. 4, *b*).

After machining, the billets were heated up to 1000 °C, kept at this temperature for 1.5 h, and then rolled with industrial scale mills via cross-rolling scheme [23]. Heat treatments, namely, annealing and strengthening STA (solution treatment and ageing), were performed in electric resistant-heating furnace in air atmosphere on the samples cut from the rolled plates. The choice of heat-treatment regimes was based on the lowest beta-transition temperature (T_β) of the alloy included in the layered material. For instance, for two-layered materials, the lowest T_b had LCB and Ti5553 alloys with 815 °C and 860 °C, respectively. In the four-layered material, c.p.Ti had the lowest T_b (850 °C).

Microstructure after different stages was examined with light (LM) and scanning electron microscopy (SEM) using OLYMPUS XL70 (Japan) and TESCAN Vega3 and Mira3 (both Czech Republic) microscopes, respectively. Local chemical compositions were determined by energy-dispersive x-ray (EDX) spectroscopy with Oxford Instruments (UK) or Bruker (Germany) devices.

Mechanical properties were studied by means of measuring Vickers hardness with Wolpert 432 SVD (Germany), and 3-point flexure with INSTRON-8802 (USA) machines. Details of testing procedures are described in Refs. [35, 36].

3. Layered Material Characterization

3.1. As-Cast State

The macrostructure of cast two-layer materials is characterized by the presence of columnar grains elongated in the vertical direction that is related to the direction of heat transfer during solidification (Fig. 5). Be-

tween the layers of alloys that differ in composition, transition zones are observed; in the case of the LCB/Ti64 material, these zones are much wider as compared to the Ti5553/Ti64 material (Fig. 5, *a vs. b*). In the 4-layered ingot, the columnar crystallites are most visible in the layer of c.p.Ti, while in both Ti64 and Ti5553 layers they are less pronounced (Fig. 5, *c*).

The microstructures of all layers were very typical for used alloys in the cast state. Ti64 layers in all cases have coarse-grain (hundreds of millimetres) lamellar microstructure (Figs. 6, *a* and *b*). The LCB microstructure was characterized by coarse β-grains, the boundaries of which were not decorated by the boundary α-phase (Fig. 6, *c*); fine acicular α-phase precipitates were observed in these grains (Fig. 6, *d*). The microstructure of Ti5553 alloy in the 4-layer material was not quite normal, *i.e.*, sections with the α-phase precipitates of different sizes were observed (Figs. 6, *e*, *f*). Most likely, this is a consequence of either the difference in temperature-kinetic solidification conditions, when the upper layers (with coarser particles of the α-phase) were formed due to slower cooling, or due to a lower concentration of alloying elements in this layer.

It should also be noted that the boundaries between the layers of different alloys in most cases looked rather broad in terms of their microstructure (Figs. 6, *g*, *h*). Only the interlayer boundary between Ti5553 and Ti64 alloys in the 4-layer ingot appeared clearly defined and narrow (Fig. 6, *i*), probably due to a certain 'favourable' crystallographic orientations of the β-grains in these areas of the adjacent layers.

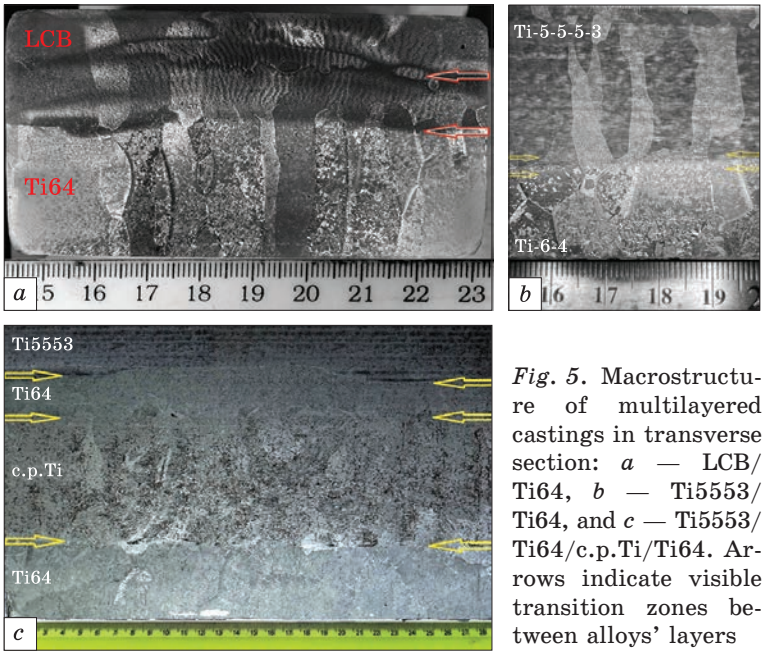

Fig. 5. Macrostructure of multilayered castings in transverse section: *a* — LCB/Ti64, *b* — Ti5553/Ti64, and *c* — Ti5553/Ti64/c.p.Ti/Ti64. Arrows indicate visible transition zones between alloys' layers

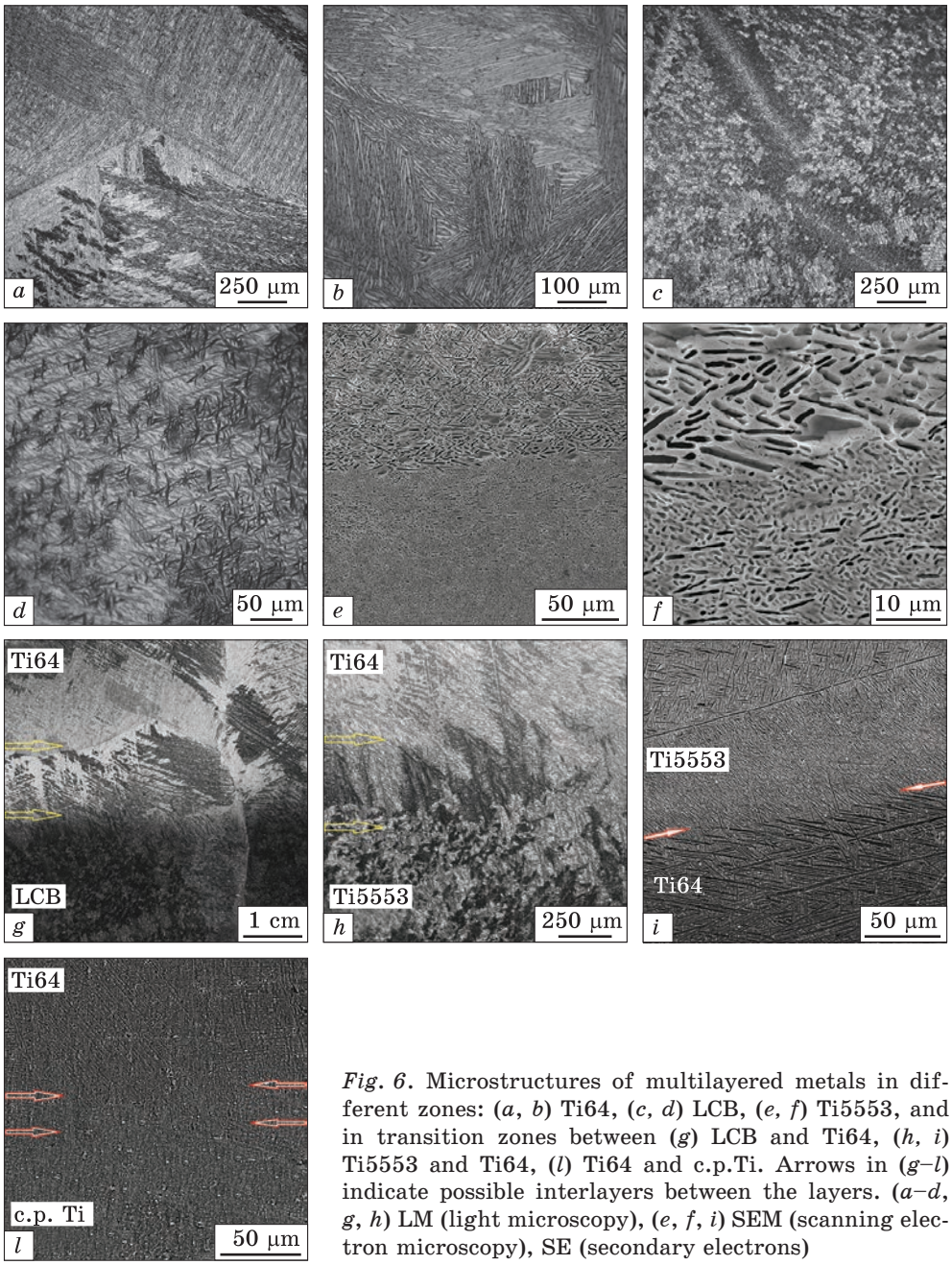

Fig. 6. Microstructures of multilayered metals in different zones: (*a*, *b*) Ti64, (*c*, *d*) LCB, (*e*, *f*) Ti5553, and in transition zones between (*g*) LCB and Ti64, (*h*, *i*) Ti5553 and Ti64, (*l*) Ti64 and c.p.Ti. Arrows in (*g*–*l*) indicate possible interlayers between the layers. (*a*–*d*, *g*, *h*) LM (light microscopy), (*e*, *f*, *i*) SEM (scanning electron microscopy), SE (secondary electrons)

The formation of relatively wide transition zones between the layers is well explained by the results of their local chemical analysis and microhardness measurements.

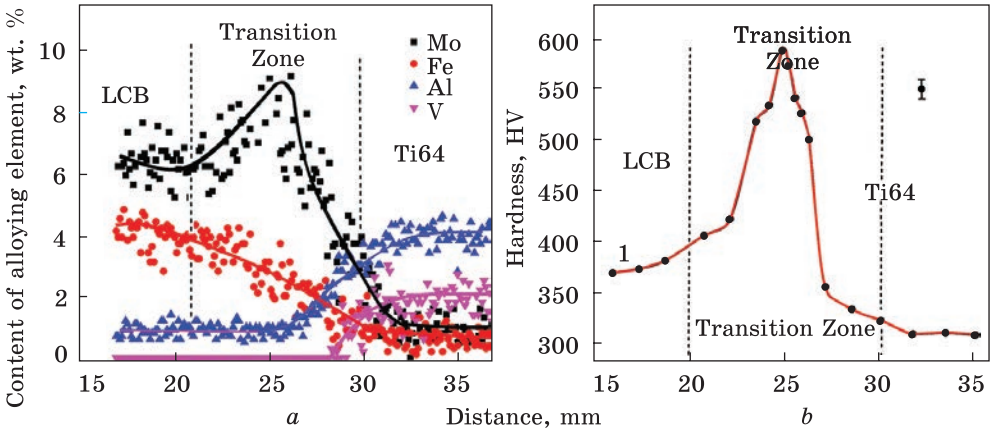

Fig. 7. Chemical elements' (*a*) and hardness (*b*) distributions within transition zone of casting between LCB and Ti64 layers

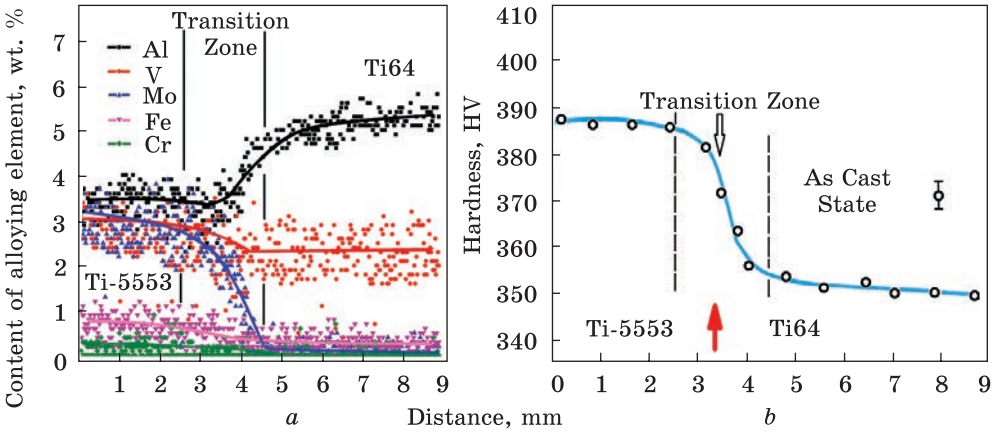

Fig. 8. Chemical elements' (*a*) and hardness (*b*) distributions within the transition zone of casting between Ti5553 and Ti64 layers

For example, in the 2-layer material Ti64/LCB, changes in the content of alloying elements, especially molybdenum (about 9 wt.%, *i.e.*, higher approximately 1.5 times), were observed in a section of about 9 mm wide (Fig. 7, *a*). Possibly, it is a result of hindered diffusion of this element across the boundary between the lower layer of Ti64 alloy and the LCB layer deposited above, when elemental metals (not master alloys) are used. As a result, this heterogeneity of the chemical composition caused a significant increase in hardness (up to 590 *HV*) approximately in the centre of the transition zone (Fig. 7, *b*).

In the case of the two-layer Ti5553/Ti64 material, due to the peculiarities of the ingot manufacturing technology (the use of pre-alloyed Ti5553 alloy instead of pure alloying elements as in the case of LCB), the

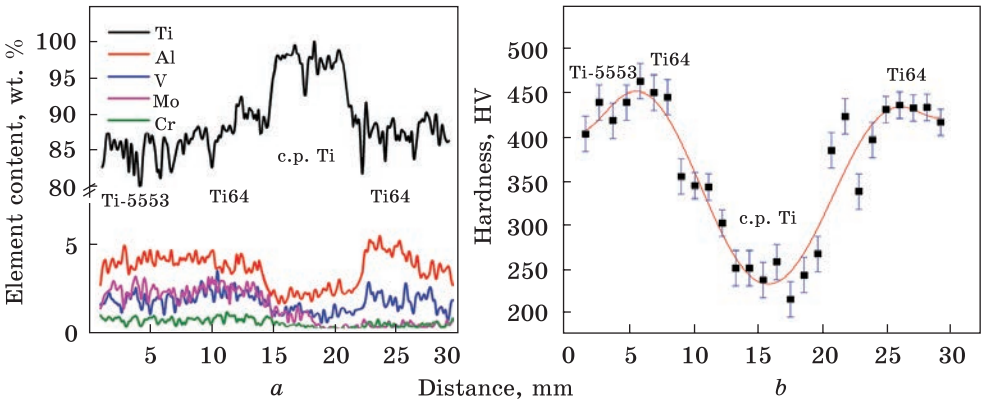

Fig. 9. Chemical elements' (*a*) and hardness (*b*) distributions in cast Ti5553/Ti64/c.p.Ti/Ti64 billet

chemical composition changed gradually on the boundary between the layers, without extrema for individual alloying elements (Fig. 8, *a*). Due to this, the hardness distribution curve in this material is also gradual, and the difference in the hardness of the Ti5553 and Ti64 layers is comparatively small (Fig. 8, *b*).

Thus, the use of pre-melted alloys as charge materials provides the production of a layered material that is more homogeneous in chemical composition in comparison with using elemental alloying elements.

Keeping this fact in mind, conventional alloys Ti64, c.p.Ti, and Ti5553 were used as initial casting materials to produce a 4-layer ingot. In the latter case, taking into account the significant evaporation of chromium during electron-beam melting, this element was additionally added following previously found dependences for various chemical elements [30, 37, 38]. The distribution of chemical elements across the cross-section of the ingot (Fig. 5, *c*) is shown in Fig. 9, *a*. The fact that the amounts of aluminium and vanadium in the neighbouring layers of Ti5553 and Ti64 (left side of Fig. 9, *a*) slightly differ is quite understandable since they are quite close in both alloys. However, a noticeable amount of molybdenum diffused into this Ti64 layer, *i.e.*, quite unexpected. At the same time, molybdenum is practically absent in the lower layer of Ti64 (right side of Fig. 9, *a*). It is also worthwhile to note a rather significant diffusion of alloying elements (first of all aluminium) from the two upper layers (Ti5553 and Ti64) into the middle layer of c.p.Ti. The hardness distribution over the cross-section of the 4-layer ingot (Fig. 9, *b*) agrees quite well with the chemical composition of the material. The minimum values (of about 220 *HV*) correspond to the c.p.Ti layer, *i.e.*, they exceed the values typical for unalloyed titanium due to the diffusion of Al, V, and Mo. The hardness of the upper (Ti5553 + Ti64) and lower (Ti64) layers is approximately twice higher than that of the c.p.Ti layer.

3.2. Rolled and Heat-Treated States

Rolling was performed with a traditional cost-efficient procedure employed for EB-melted titanium materials [23–26, 28, 30]. It consisted of a furnace heating up to 1050 °C that was close to the beta-transition T_β (the temperature of the polymorphous $\alpha + \beta_0 \rightarrow \beta$-transformation [2]) for Ti64 alloy (the highest one among the alloys used) and exposure for at least 1 hour. Since all alloys were in an as-cast state and had coarse β-grains before deformation, such furnace heating did not lead to additional coarsening of the grains. Heated billets were cross-rolled to a final 14 mm thickness. Number of rolling passes was varied from 6 to 9, depending on the hot stiffness of the material. A typical example of the rolled plate is shown in Fig. 10.

The regimes of the heat treatments were chosen also based on the T_β temperatures of the alloys present in each layered specimen. Two types of heat treatments were used: (i) annealing aimed at stabilization of phase compositions and microstructures, and (ii) strengthening with so-called

Fig. 10. General view of rolled bilayer plates from (*a*) Ti64, and (*b*) LCB sides, and (*c*) 4-layers plate from Ti5553 side

Table 1. **States of layered materials as objects of the studying the micro-structure, chemical compositions, and some properties (FC—furnace cooling, STA—solution treatment and ageing, WQ—water quenching)**

No	Materials	Treatment
1 2 3	LCB/Ti64	As-rolled + + Annealing (800 °C, 2 h, FC) + + STA (840 °C, 1 h, WQ) + Ageing (538 °C, 6 h)
4 5 6 7	Ti5553/Ti64	As-rolled + + Annealing (800 °C, 2 h, FC) + + STA (850 °C, 1 h, WQ) + Ageing (538 °C, 10 min) + + STA (850 °C, 1 h, WQ) + Ageing (538 °C, 6 h)
8 9 10	Ti5553/Ti64/c.p.Ti/Ti64	As-rolled + + Annealing (800 °C, 2 h, FC) + + STA (850 °C, 1 h, WQ) + Ageing (600 °C, 6 h)

solution treatment and ageing. All states investigated and treatments employed are listed in Table 1.

3.2.1. Two-Layer LCB/Ti64 Material

In the as-rolled state, this two-layer material had a wider zone between the LCB and Ti64 layers than in the as-cast state (especially compared to the plate thickness of 14 mm) (Fig. 11). Moreover, within this zone, some lamination was observed in both the fine microstructure and the distribution of alloying elements (Figs. 11, *b* and *c*). First of all, this applies to Mo, the maximum peak of which increased to almost 20 wt.% (*cf.* Figs. 11, *c* and 7, *a*). This change in the chemical composition of the material as a result of rolling (hot deformation) looks very unusual. The phenomenon of uphill diffusion has already been observed under some specific conditions of external impact [37, 38], including deformation and increased temperatures. Because of such a change in the chemical composition, the phase

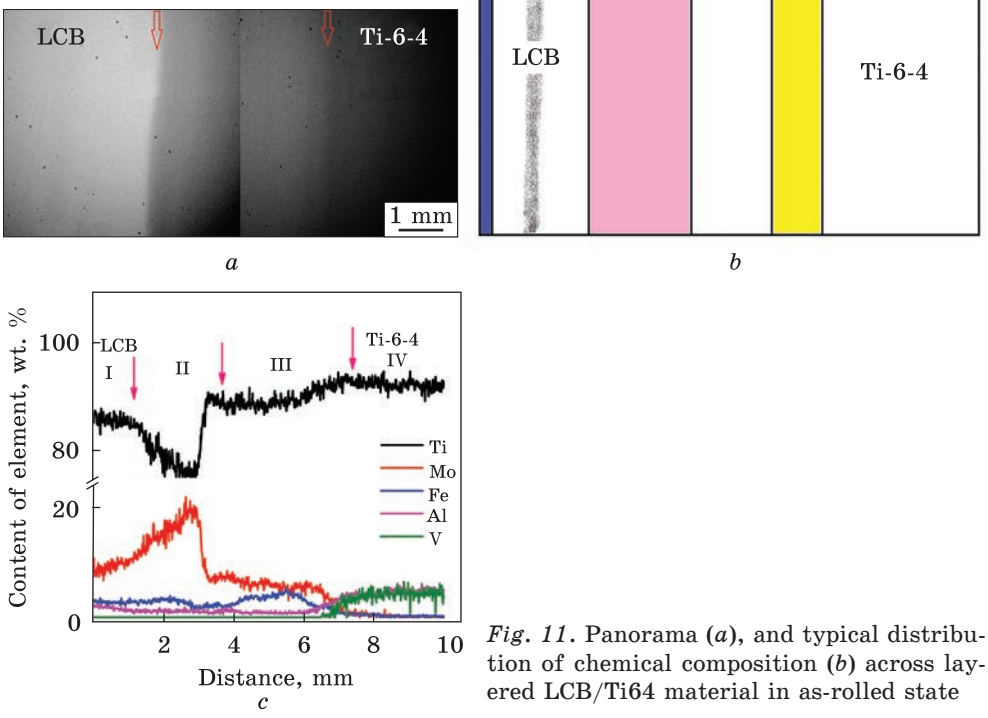

Fig. 11. Panorama (*a*), and typical distribution of chemical composition (*b*) across layered LCB/Ti64 material in as-rolled state

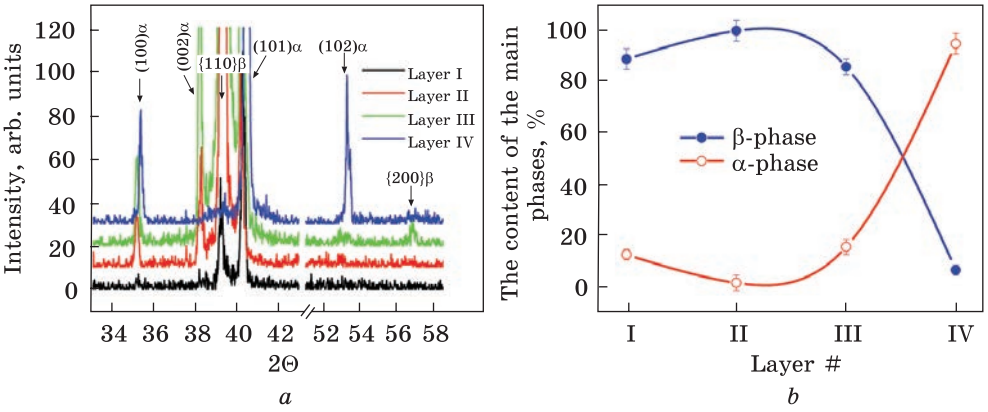

Fig. 12. X-ray diffraction patterns from different layers of LCB/Ti64 material in as-rolled state (*a*) and amount of phases in layers (*b*) calculated based on the XRD data

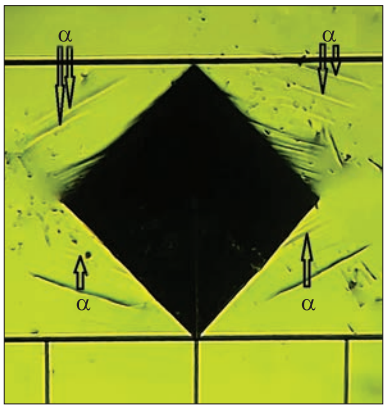

Fig. 13. Martensite needles appeared upon hardness test in transition layer (II in Figs. 11 and 12)

composition of these layers turned out to be quite expected. Fig. 12 shows the results of layer-by-layer x-ray diffraction analysis (Fig. 12, *a*) and calculated fractions of the β- and α-phases (Fig. 12, *b*) in the LCB/Ti64 material after rolling. Thus, the metastable β-phase predominates in the zones I–III where strain-induced α″-martensite forms even during hardness measuring (*i.e.*, under plastic deformation caused by indentation of a diamond pyramid), what is typical for such concentrations of β-phase stabilizing alloying elements [39].

Fine microstructure of bi-layered LCB/Ti64 material in an as-rolled state (Figs. 14, *a*–*g*) had the α-phase non-uniform both in morphology and size, as well as in its amount in local zones. As we move from the surface into the bulk, relatively coarse plates/needles of the α-phase (Fig. 14, *a*) are first replaced by finer particles (Fig. 14, *b*) which become fewer and fewer (Fig. 14, *c*), and even a field of the α-phase free of them appears (Fig. 14, *d*). Further, the density of fine α-particles increases again (Fig. 14, *e*). Then, with a gradual transition to the Ti64 layer (Fig. 14, *f*), the microstructure becomes coarse-lamellar, *i.e.*, is typical for this alloy (Fig. 14, *g*).

Subsequent annealing at 800 °C (see Table 1) caused decomposition of the metastable β-phase and stabilization of α + β-phase composition, namely, the microstructure is finer in the LCB layer (Figs. 14, *h* and *i*) and

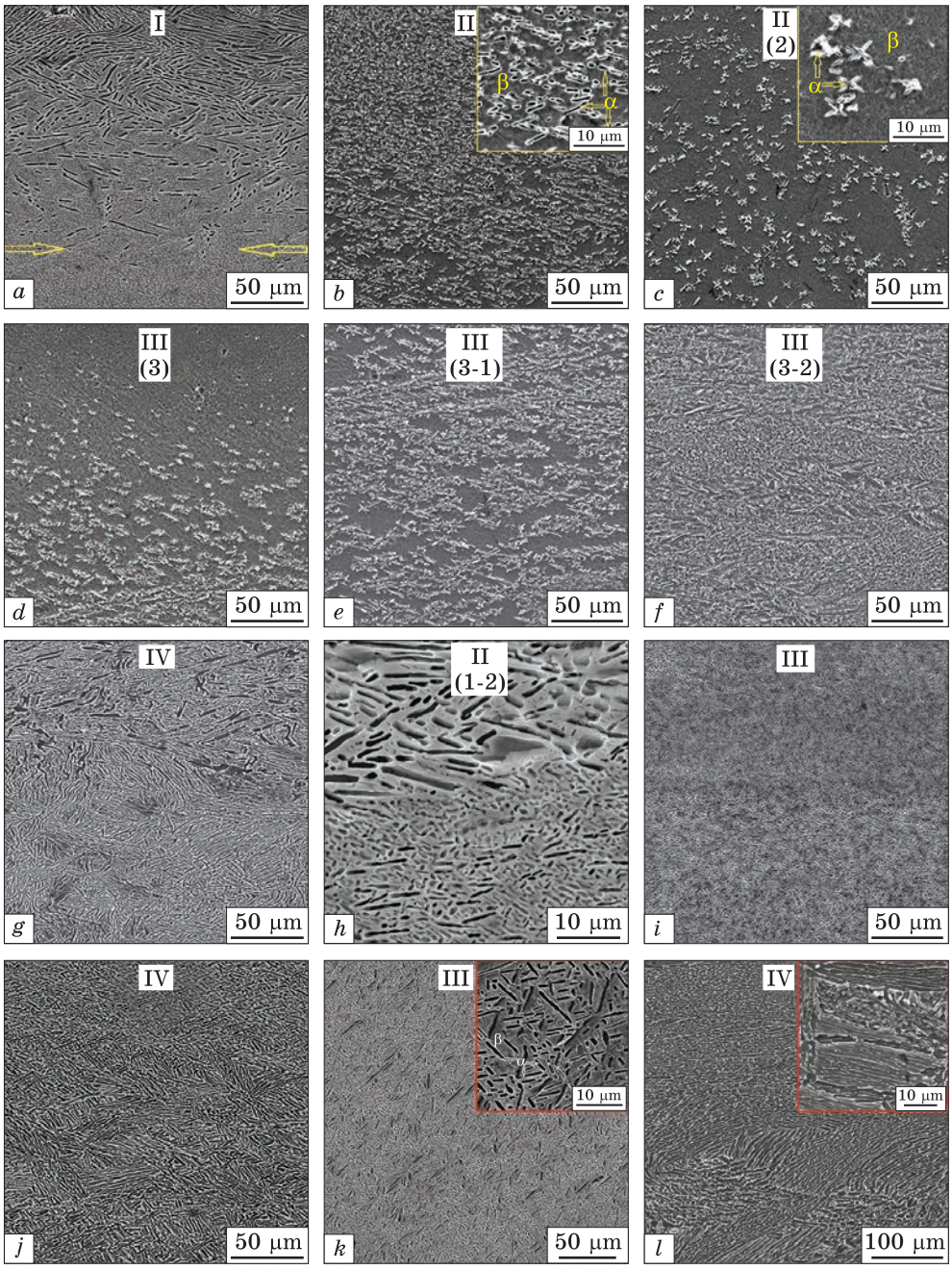

Fig. 14. Microstructure (layer-by-layer) of LCB/Ti64 material in as-rolled (*a*–*g*), annealed (*h*–*j*), and STA-hardened (*k*, *l*) states in locations (numbers (I), (II), *etc.* according scheme in Fig. 11, *b*). SEM, (*a*, *h*, *k*) SE, (*b*–*g*, *i*, *j*, *l*) BSE (backscattered electrons)

coarser in the Ti64 layer (Fig. 14, *j*). The boundary between these layers is not clearly visible (Fig. 14, *i*). STA hardening heat treatment (*ibid*) resulted in almost the same microstructure of the LCB (Fig. 14, *k*) and Ti64 (Fig. 14, *l*) layers.

It can be noted that the traces of deformation such as twisted coarse α-plates are observed after both heat treatments (Figs. 14, *a*, *g*, *j*, and *l*). This fact indicates that the deformation applied upon rolling, and heating during subsequent heat treatments did not provide conditions enough for the recrystallization of the phases in this bimetal.

3.2.2. Two-Layer Ti5553/Ti64 Material

As was shown above for as-cast state, the two-layer Ti5553/Ti64 material had no extrema in the distribution of alloying elements; due to this, the boundary between the layers was smooth (Fig. 8). This situation still the same after rolling; the α-phase crystallites in both layers of Ti5553 and Ti64 became significantly finer (compare Figs. 15, *a*, *b* with Figs. 6, *a*, *b*, and Figs. 6, *h*, *i*), and the boundary between these layers was smooth, very uniform and rather indistinct (Fig. 15, *c*). Primary α-phase and β-phase were well seen in both layers, but the amount of the latter was higher for stable equilibrium conditions of these alloys, which indicates that the material was cooled rapidly enough from the rolling temperature, so a metastable state of the phases was fixed.

Annealing resulted in some coarsening of the α-phase plates (see Figs. 15, *d* and *e vs.* Fig. 15, *a*; Figs. 15, *f* and *g vs.* Fig. 15, *b* for Ti5553 and Ti64 layers, respectively). It can be noted that in this material, similar to the LCB\Ti64 material, complete recrystallization of the α-phase did not occur, *i.e.*, grain boundaries curved by deformation are observed in the Ti64 layer (Fig. 15, *f*).

The strengthening STA heat treatment significantly changed the microstructure of the material (Fig. 15, *h*). As a result, a bimodal microstructure was formed in both layers, consisting of primary, relatively coarse crystallites of the α-phase (α_{pr}) and a fine mixture of secondary α (α_{sec}) and β phases between them (Figs. 15, *i*, *j*). The aspect ratio between the primary α-phase and the β-transformed α+β-mixture is small; however, this made it possible to somewhat increase the hardness of these layers as will be shown below.

3.2.3. Four-Layer Ti5553/Ti64 Material

In the Ti5553 and Ti64 layers of the 4-layered material, the changes in the microstructure both after rolling and after all heat treatments were like the above-described case of the 2-layered material. As some differences, one can note the rather wide and 'winding' boundary between the Ti5553 and Ti64 layers (Fig. 16, *a*, *b*), as well as the boundary between the c.p.Ti

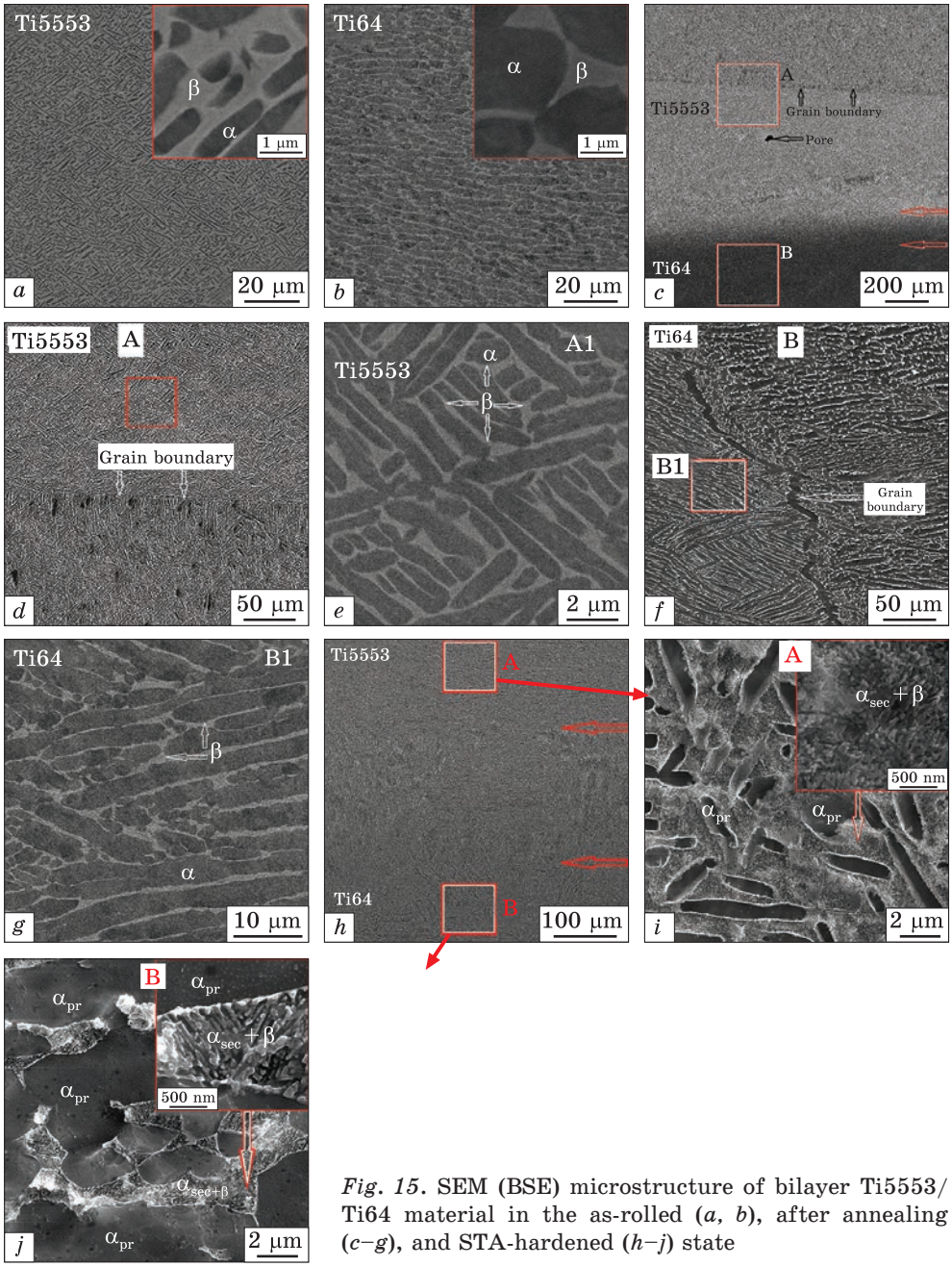

Fig. 15. SEM (BSE) microstructure of bilayer Ti5553/Ti64 material in the as-rolled (*a*, *b*), after annealing (*c*–*g*), and STA-hardened (*h*–*j*) state

and Ti64 layers, which is rather difficult to distinct due to poor etchability (Fig. 16, *c*). Such broadening of boundaries can be explained by the diffusion of alloying elements, which was quite active and over relatively

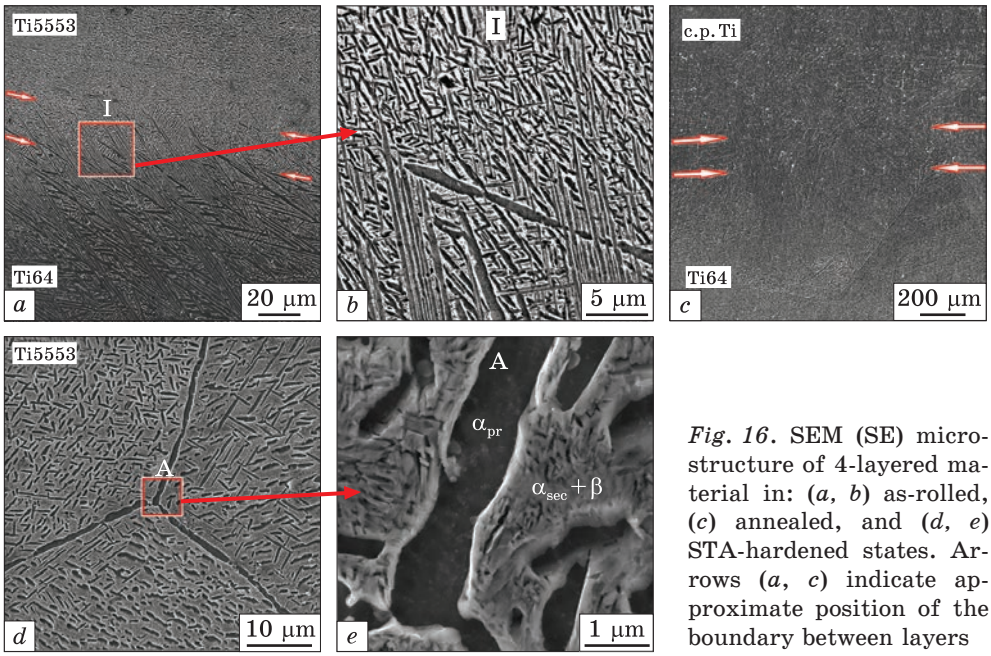

Fig. 16. SEM (SE) microstructure of 4-layered material in: (*a*, *b*) as-rolled, (*c*) annealed, and (*d*, *e*) STA-hardened states. Arrows (*a*, *c*) indicate approximate position of the boundary between layers

large distances (see Fig. 9, *a*). It is also possible to note somewhat larger sizes of particles of the primary α-phase (α_{pr}) in the STA-hardened layer of Ti5553 (Figs. 16, *d* and *e*). The most probable reason for this is the longer time the material was exposed to high temperatures since the melting time of the 4-layered material was longer than that of the 2-layered ones.

4. Mechanical Behaviour

4.1. Hardness

Figure 17 shows the results of hardness tests performed with layered materials in different states, namely, in as-cast, rolled, after annealing, and after STA-hardening treatments. The presented data allow tracing of how the hardness distribution profile changed due to deformation and subsequent heat treatments. In the LCB/Ti64 material, rolling followed by annealing led to a significant decrease in hardness in all areas, *i.e.*, both in both layers and in the transition zone between them (Fig. 17, *a*, curve *2 vs.* curve *1*). STA-hardening heat treatment, as expected, increased hardness in all zones (Fig. 17, *a*, curve *3*), but its level remained lower than in the initial as-cast state.

In the two-layered Ti5553/Ti64 material, hardness measurements were made on a larger number of variants of microstructural states. Fig. 17, *b* presents changes in hardness around the conventional central line in the middle of the transition zone between Ti5553 and Ti64 alloys. From a

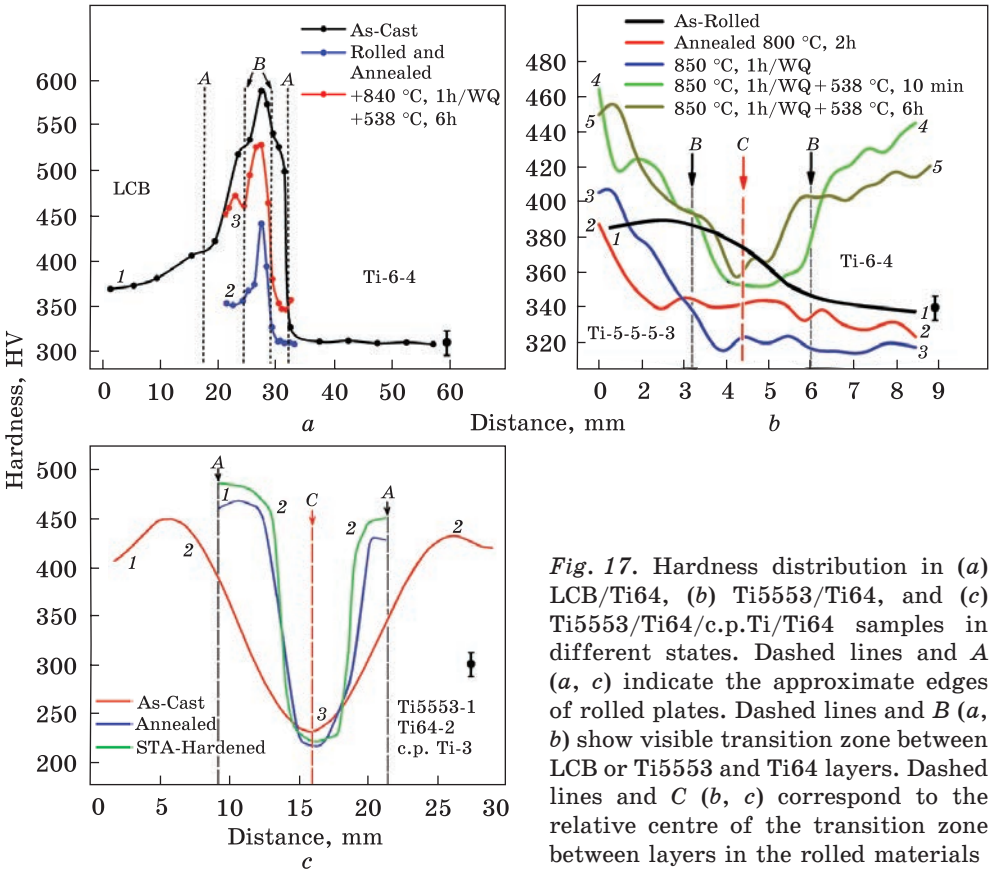

Fig. 17. Hardness distribution in (*a*) LCB/Ti64, (*b*) Ti5553/Ti64, and (*c*) Ti5553/Ti64/c.p.Ti/Ti64 samples in different states. Dashed lines and *A* (*a*, *c*) indicate the approximate edges of rolled plates. Dashed lines and *B* (*a*, *b*) show visible transition zone between LCB or Ti5553 and Ti64 layers. Dashed lines and *C* (*b*, *c*) correspond to the relative centre of the transition zone between layers in the rolled materials

comparison of these data, it can be concluded that in the as-rolled condition, the hardness smoothly changes from 380–390 *HV* in the Ti5553 layer to 340 *HV* in the Ti64 layer (Fig. 17, *b*, curve *1*), which indicates approximately the same work hardening of both layers. Annealing (800 °C, 2 h; curve *2*, *ibid.*) led to the relaxation of defects; metastable phases appeared upon deformation and formed stable and relatively softer α+β-structure. Solid solution treatment (850 °C, 1 h) also caused relaxation of all deformation defects, and after water quenching it caused some softening of the material except the very top layer of Ti5553, depleted of β-stabilizing elements and probably additionally saturated with oxygen and nitrogen (Fig. 17, *b*, curve *3*). Additional ageing at 538 °C (usually applied for alloys like Ti5553 [40]) was performed in two ways: (i) with very short isothermal exposure for 10 min, which could provide the highest strength due to the realization of earlier stages of metastable β-phase decomposition and precipitation of fine and hard ω-particles [39], and (ii) 6-hour ageing forming less strong, but stable α+β-state (see Figs. 15j and 16, *e*). However, such a difference in the ageing modes did not result in a notice-

able difference in the hardness of both alloys (Fig. 17, *b*, curves *4* and *5*). This negative result is apparently a consequence of either too low heating temperature for quenching or insufficient content of alloying elements in the Ti55553 layer due to their diffusion into the transition zone (see Fig. 8, *a*). Nevertheless, both ageing modes allowed an increase in the hardness of both layers of alloys to an average of 420–440 *HV*.

Unexpectedly, the most complex in its composition 4-layer material had the smoothest dependencies of hardness distribution across the cross-section (Fig. 17, *c*). Another unexpected effect is that rolling and subsequent heat treatments had minimal effect on the hardness level on both sides of the material (curves *2* and *3 vs.* curve *1*), while in the centre (c.p.Ti) the hardness was unchanged at about 220 *HV*.

The general conclusion of the analysis of the curves presented in Fig. 17 is that the applied technological approach allowed the production of layered materials with variable hardness, and hardness changed in two ways. In the first material (LSB/Ti64), the hardest layer (up to ≈580 *HV*) is in the centre of the plate and is surrounded on both sides by softer layers with a hardness of 370 and 310 *HV*. The other two materials have a softer core, and in the case of Ti5553/Ti64 the difference between the edges and the centre is not too big (≈90 *HV*). In the case of the 4-layered material, the difference is quite large: the c.p.Ti centre has a little more than 200 *HV*, while at the edges the hardness can reach more than 450 *HV*.

4.2. Three-Point Flexure

It was quite expected that the presence of layers differing in composition and hardness would influence in a certain way other properties of the layered materials. Figure 18 shows some results of 3-point flexure tests of Ti5553/Ti64 material in two conditions, after annealing and in the STA-strengthened state, under loading applied on both sides. The curves' comparison clearly shows that the main difference between these two structural states is their ductility. In the annealed state, ductility is significantly higher. When a bending load from the Ti64 alloy (curve *2* in Fig. 18) is applied, both maximum strength (2110 MPa) and ductility (deflection of 15.3% with plastic transition to frac-

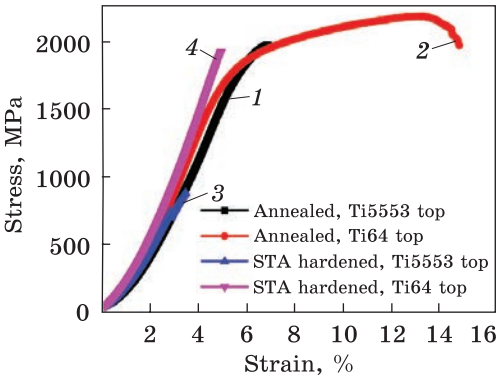

Fig. 18. 3-point flexure of 2-layer Ti5553/Ti64 material in the annealed (*1*, *2*) and STA-hardened (*3*, *4*) states tested with load applied from Ti5553 (*1*, *3*) and Ti64 (*2*, *4*) sides. Strain rate 10^{-2} s^{-1}

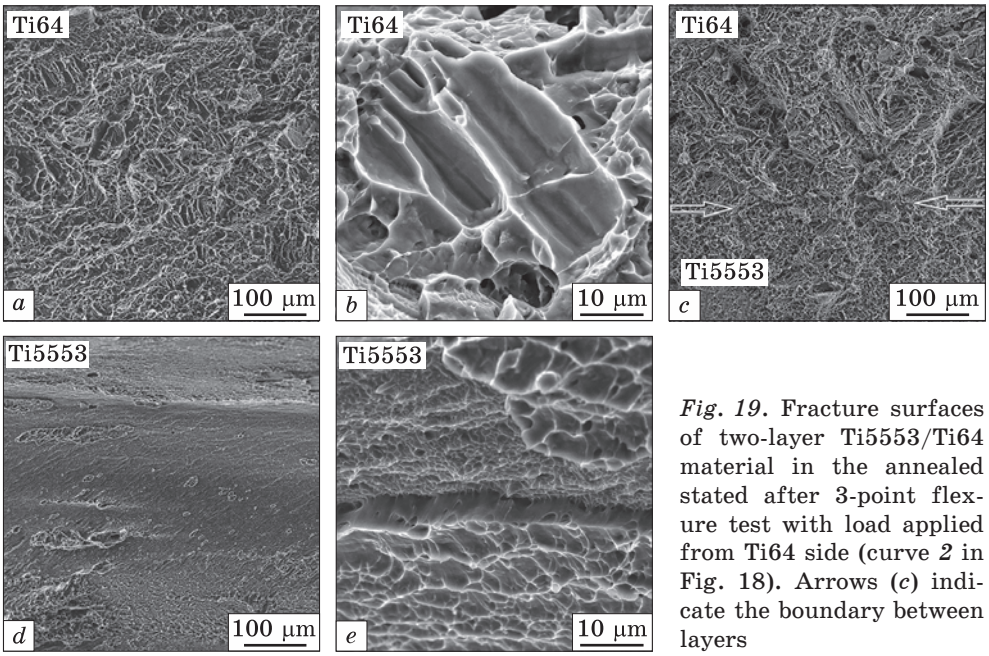

Fig. 19. Fracture surfaces of two-layer Ti5553/Ti64 material in the annealed stated after 3-point flexure test with load applied from Ti64 side (curve *2* in Fig. 18). Arrows (*c*) indicate the boundary between layers

ture) are achieved. When the load was applied from the reverse side of Ti5553, the sample fractured almost immediately after the beginning of plastic deformation (curve *1 ibid.*). The samples in STA-hardened state in both cases (load applied from both sides) fractured at the stage of elastic deformation, and the fracture occurred at earlier stages when the load was applied on the Ti5553 side (curve *3 vs.* curve *4*, *ibid.*).

An explanation for this behaviour of the layered materials can be found by comparing the standard characteristics of these alloys tested by bending and by analysing the fracture surfaces of the tested specimens. For example, the Ti64 alloy in the annealed state, depending on the type and dispersion of the microstructure, had strength of ≈900 MPa and ductility (relative elongation) within the range of 10–20% under tensile tests [2, 41]. Under 3-point bending, the strength was 1900 MPa, but flexure strain varied from 10 to 25% [35]. More alloyed and hard Ti5553 alloy even in the annealed state had strength of 1050 MPa and an elongation of about 10–14% [41–45]. No data on 3-point bending tests for Ti5553 alloy in the annealed $\alpha + \beta$-condition were found in the literature. However, considering the general relationship between tensile and bending properties, it can be assumed that the 3-point bending strength of Ti5553 could exceed 2000 MPa. Thus, the main difference between the two alloy layers is their strength.

The fracture surface of the tested Ti64/Ti5553 sample in an annealed state after loading on the Ti64 side is presented in Fig. 19. The surface of

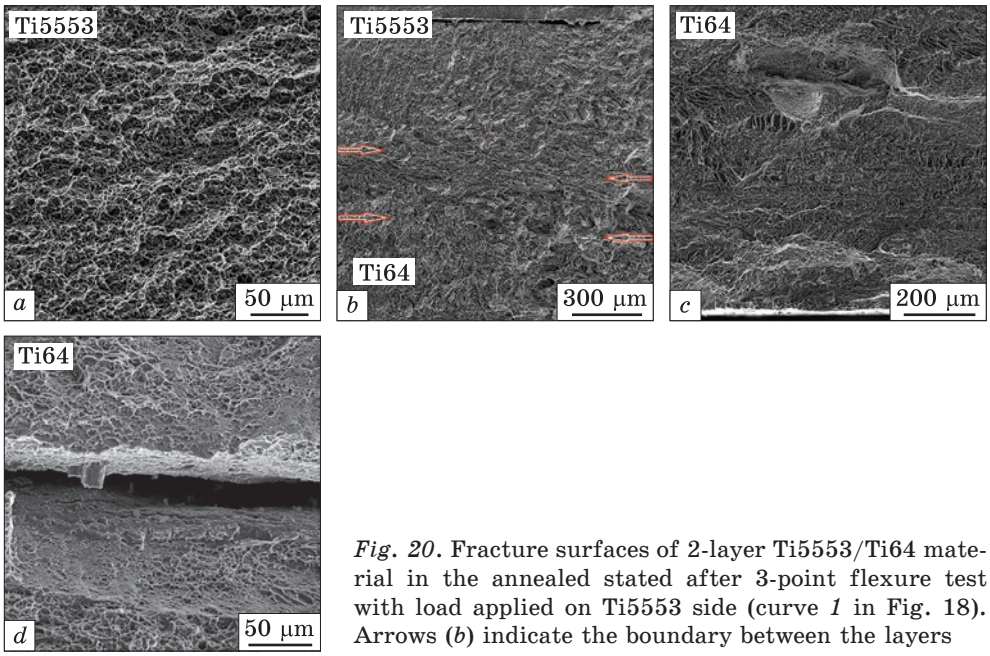

Fig. 20. Fracture surfaces of 2-layer Ti5553/Ti64 material in the annealed stated after 3-point flexure test with load applied on Ti5553 side (curve *1* in Fig. 18). Arrows (*b*) indicate the boundary between the layers

the Ti64 layer had a ductile fracture pattern with dimples (Fig. 19, *a*). The dimples repeated the shape of the α-phase lamellas (Fig. 19, *b*). The boundary between the layers remained smooth and did not have any special features (Fig. 19, *c*). The surface of the Ti5553 layer appears flatter with pronounced banding, probably reflecting the metal layers deposited during the melting process (Fig. 19, *d*). At higher magnification, it becomes clear that at the micro-level this layer also fractured ductile (Fig. 19, *e*).

Comparing these results with the data on the mechanical properties of the two alloys and taking into account the loading scheme, we can come to the following conclusion. Applying a bending load to the softer Ti64 layer (which is subjected mainly to compressive stresses [33]) results in the greatest tensile stress acting on the lower Ti56553 layer. This lower Ti5553 layer is deformed until it reaches its maximum strength, after which a main crack appears in it, which propagates upward until the entire sample is completely fractured.

A different situation occurs in the case of application of bending load on the Ti5553 layer, when the maximum tensile stresses arise in the lower, less strong Ti64 layer (Fig. 20). Despite the character of fracture was still ductile on the micro-level in both layers (Figs. 20, *a*, *c*), and boundary between them did not make any visible influence (Fig. 20, *b*), some delamination took place inside the Ti64 layer (Fig. 20, *d*). Obviously, the fact that Ti64 has lower strength than Ti5553 caused earlier fracture of this layered material as compared to the previous case (*cf.* curves *1* and *2* in Fig. 18).

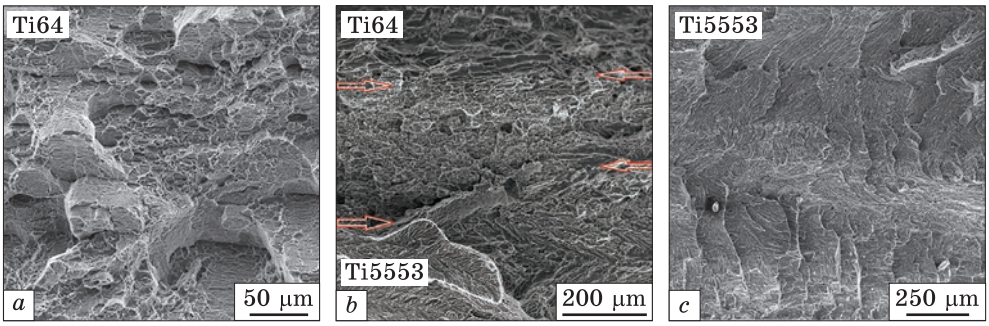

Fig. 21. Fracture surfaces of 2-layer Ti5553/Ti64 material in the STA-strengthened stated after 3-point flexure test with load applied on Ti64 side (curve *4* in Fig. 18). Arrows (*b*) indicate the boundary between the layers

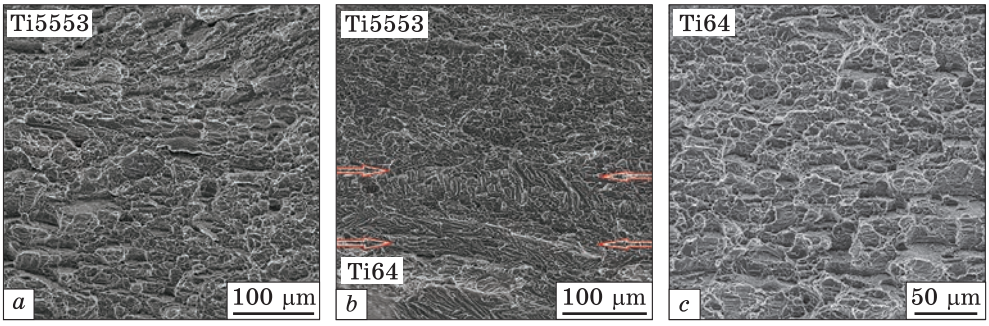

Fig. 22. Fracture surfaces of 2-layer Ti5553/Ti64 material in the STA-strengthened stated after 3-point flexure test with load applied on Ti5553 side (curve *3* in Fig. 18). Arrows (*b*) indicate the boundary between the layers

After the STA-hardening heat treatment even with a 'soft' regime (No. 7 in Table 1), the tensile strength of both materials increased: for Ti64, up to approximately 1100 MPa, and for Ti5553, up to ≈1250 MPa [2, 41]. As a result, the character of the fracture surfaces changed drastically (Figs. 21, and 22). In both cases, when the load was applied on Ti64 or Ti5553 sides, the fracture was brittle with evidence of cracks' propagation along the β-grain boundaries (Figs. 21, *a*, *b*) or subgrains (α-packets colonies inside β-grains, Figs. 22, *a*–*c*). This fact indicates that the interior volume of β-grains is stronger than the grain-boundary α-phase after hardening [2, 42, 46]. In this STA-hardened state, the interlayer between two alloys affects the deformation and cracking of the sample (Figs. 21, *b* and 22, *b*). Finally, such embrittlement led to the very early fracture of layered material on the stage of elastic deformation (curves 3 and 4 in Fig. 18). Like in the case of the annealed state, the specimen in which load was applied on a stronger Ti5553 side fractured earlier in the hardened state (curve *3*, *ibid.*).

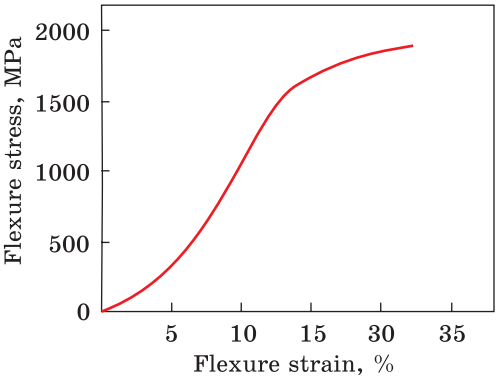

a

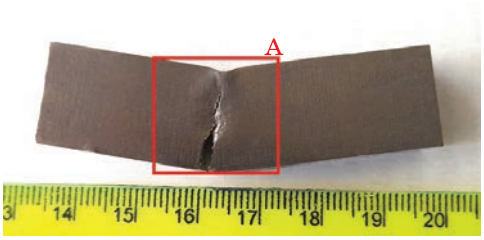

b

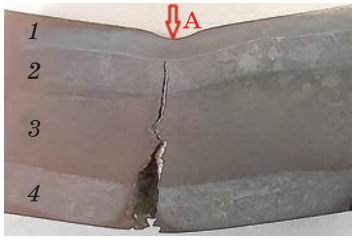

c

Fig. 23. The stress–strain curve for 4-layered sample in the annealed (800 °C, 2 h) state for the 3-point test with strain rate 10^{-2} s^{-1} (*a*), and sample after the test (*b*, *c*). *1*, *2*, *3*, *4* layers (*c*) indicate Ti5553, Ti64, c.p.Ti, Ti64, respectively. The arrow (*c*) indicates a place of applying the bending force

The test of the 4-layer sample also showed a very interesting result. Figure 23 shows the stress–strain curve (*a*) and the appearance of the sample after the test (*b*). Comparing this curve with similar data for the 2-layer Ti5553/Ti64 material (Fig. 18), it is possible to conclude that strength characteristics (yield strength (YS) is 1522 MPa, ultimate tensile strength (UTS) is 1903 MPa) are a little bit lower in the case of the 4-layered sample. However, ductility (flexure strain) is at least 7% higher. Moreover, unlike all 2-layer samples, the 4-layer one did not break (Fig. 23, *b*). Additionally, it should be noted that the crack visually was stopped on the boundary between the top Ti64 and lower Ti5553 layer, and the end of the crack is slightly deviated from the point of application of the bending force (Fig. 23, *c*).

SEM observations of fine microstructure revealed a crack stop in the upper Ti5553 layer (Fig. 24, *a*, *b*). The end of the crack is a network of small cracks distributed over fine elements of the microstructure, probably colonies of α-plates (Fig. 24, *b*). The first wide expansion of the main crack with a sharp change in its direction is observed at the boundary between the Ti64 and Ti5553 layers (Fig. 24, *c* and *d*). However, the crack branches and opens most widely earlier within the middle layer of the c.p.Ti (Fig. 24, *a*). At the boundary between the Ti64 and c.p.Ti layers, a fairly fine-dimple relief is visible on the crack surface, which repeats the α + β structure of the two-phase alloy (Fig. 24, *e*). Inside the c.p.Ti layer

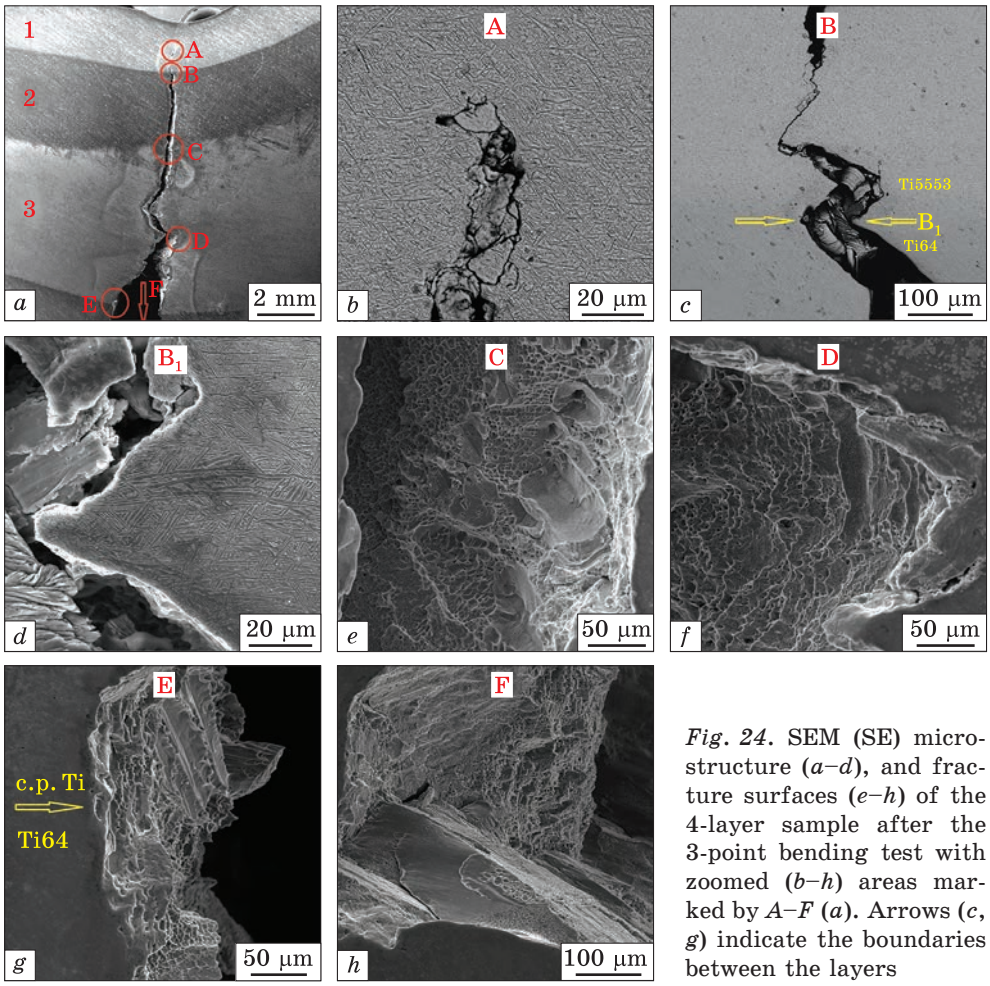

Fig. 24. SEM (SE) microstructure (*a*–*d*), and fracture surfaces (*e*–*h*) of the 4-layer sample after the 3-point bending test with zoomed (*b*–*h*) areas marked by *A*–*F* (*a*). Arrows (*c*, *g*) indicate the boundaries between the layers

itself, the dimples are somewhat coarser (Fig. 24, *f*). The sharp change in the direction of crack propagation in this layer is most likely due to the structure of the metal deposited layer-by-layer and a greater distance of the influence of the stresses around the crack tip in the less strong metal [47]. At the boundary between the c.p.Ti and the lower Ti64 layer, fracture traces repeating the elements of the two-phase microstructure appear again (Fig. 24, *g*). In the lowest Ti64 layer, from where the crack began to grow, cleavage planes are visible (Fig. 24, *h*), which is a sign of the fairly rapid 'explosive' nature of the crack initiation and early growth.

Thus, summarizing the results of the study of this 4-layer material after 3-point bending tests, we can conclude the following. At the initial stage of deformation, the two upper layers of Ti5553 and Ti64 are deformed by compression, while the middle layer of c.p.Ti and, especially,

the bottom Ti64 layer are deformed by tension. C.p.Ti is the most ductile with the lowest level of yield strength, but the tensile strain is the highest in the bottom Ti64 layer. When the strength limit is reached in this Ti64 layer, a crack explosively forms, and very quickly penetrates deep into the c.p.Ti layer above it, since the stress in this unalloyed titanium layer already significantly exceeds the yield limit and metal is intensely deformed plastically. When approaching the stronger Ti64 layer and, then, the Ti5553 layer, the crack somewhat slows down, and the boundaries between the layers slightly change the direction of growth.

4.3. Comparison with Other Layered Titanium Materials

Currently, titanium-based laminated materials are produced mainly by a few different technologies, first of all, different cladding methods, and powder metallurgy [6, 9, 48–53]. Among cladding technologies, explosion welding attracts the greatest interest, as it allows not only joining titanium alloys of different chemical compositions [47] but also titanium with steels [49, 50]. Titanium coating on steel is used to protect port and offshore structures from corrosion in seawater [53]. However, the main purpose of such layered materials' application is to use them as elements of armour protection [50–52].

Comparing titanium-based layered materials with each other is quite difficult since they differ in a large number of parameters — composition, structure, and manufacturing methods. First of all, this concerns the comparison of their mechanical characteristics. In most cases described in the literature, low-alloy titanium alloys were joined, when the maximum hardness on the Ti64 side did not exceed 340 *HV* [50]. A slightly higher hardness (400 *HV*) was reached in the transition layer between c.p.Ti and low-alloy steel when joining by vacuum rolling due to the formation of a diffusion zone enriched with iron [52, 57]. However, the presence of a steel layer in the material significantly increases the overall specific weight of the material. The higher hardness values can be achieved by introducing high-modulus particles (like carbides of borides) into the titanium matrix [53–56]. Such an approach allows enhancing hardness up to 800–1000 *HV* and higher, with rather good ductility of the matrix [53, 58]. The main methods for manufacturing such composites are additive technologies: powder metallurgy and 3*D*-printing. This combination of characteristics provides several unique properties, such as armour resistance.

However, if we compare the various methods of manufacturing multilayer titanium material in terms of their ease of manufacture and process productivity, then we can set quite clear priorities. For example, the use of powder metallurgy methods requires the production of specialized press forms, the use of powerful pressing equipment and high-vacuum high-temperature furnaces. The consequence of this is the complexity and mul-

tistage nature of the technology, as well as the fairly high cost of the final products, especially in small-scale production. Approximately the same problems, namely relatively low productivity and high cost, also apply to most 3*D*-printing technologies, especially those based on the use of expensive pre-alloyed powders and lasers as sources of heating. At the same time, the electron-beam melting considered in this paper is a very productive and effective technique for smelting titanium alloys. As was shown earlier, the use of this technique for producing titanium ingots in combination with subsequent rolling with one heating provides the most economical way to produce rolled Ti64 alloy suitable for use as armour material for battlefield vehicles [23, 24]. Electron-beam melting allows the production of ingots weighing several tons in one cycle, which is unachievable with any of the additive techniques. Besides, the presence of an intermediate cold hearth in the equipment allows the production of layered materials directly during the melting process, which is unachievable with other melting methods, such as vacuum arc melting with consumable electrodes.

5. Summary

Electron-beam melting can be successfully used to manufacture multilayer materials based on titanium and its alloys. This technique allows producing materials that combine layers that differ in composition, structure and properties, with good adhesion between them. Such layered materials have special properties. The choice of their composition, as well as the methods of thermomechanical and thermal treatment after melting and solidification, should be done based on the features of the subsequent use of these materials.

Acknowledgements. The research and works carried out at G.V. Kurdyumov Institute for Metal Physics of the N.A.S. of Ukraine were funded by the National Academy of Sciences of Ukraine within the budget projects КПКВК 6541230 (State Reg. No. 0123U100898) for 2023–2024 and КПКВК 6541030 (No. 060/23) for 2023–2027. The investigation and works performed at E.O. Paton Electric Welding Institute of the N.A.S. of Ukraine were funded by the National Academy of Sciences of Ukraine within the budget project No. 30.57.21/37.

REFERENCES

1. U. Zwicker, *Titan und Titanlegierungen* (Berlin: Springer-Verlag: 1974); https://doi.org/10.1007/978-3-642-80587-5
2. G. Luetjering and J.C. Williams, *Titanium* (Berlin: Springer: 2007); https://doi.org/10.1007/978-3-540-73036-1
3. M. Peters, J. Kumpfert, C.H. Ward, and C. Leyens, *Adv. Eng. Mater.* **5**, No. 6: 419–427 (2003); https://doi.org/10.1002/adem.200310095

4. J.H. Bernt and M.S. Persson, *Ballistic Protection Plate of Titanium with Layered Properties* (2008), European patent application EP 1935995A1.
5. J.K. Lee, *Analysis of Multi-Layered Materials under High Velocity Impact Using CTH* (Theses for Master of Science in Aeronautical Engineering) (Ohio: Air Force Institute of Technology: 2008);
https://scholar.afit.edu/etd/2685
6. P.E. Markovsky, D.G. Savvakin, O.O. Stasiuk, S.H. Sedov, V.A. Golub, D.V. Kovalchuk, and S.V. Prikhodko, *Metallofiz. Noveishie Tekhnol.*, **43, No.** 12: 1573–1588 (2021);
https://doi.org/10.15407/mfint.43.12.1573
7. P. Ranaweera, D. Weerasinghe, P. Fernando, S.N. Raman, and D. Mohotti, *Int. J. Prot. Struct.*, **11**, No. 3: 379–410 (2020);
https://doi.org/10.1177/2041419619898693
8. G. Ben-Dor, A. Dubinsky, and T. Elperin, *Theor. Appl. Fract. Mech.*, **88**: 1–8 (2017);
https://doi.org/10.1016/j.tafmec.2016.11.002
9. O.M. Ivasishin, P.E. Markovsky, D.G. Savvakin, O.O. Stasiuk, M.N. Rad, and S.V. Prikhodko, *J. Mater. Process. Technol.*, **269**: 172–181 (2019);
https://doi.org/10.1016/j.jmatprotec.2019.02.006
10. S.L. Semiatin and I.M. Sukonnik, Rapid heat treatment of titanium alloys, *Symposium on Physical Simulation of Casting, Hot Rolling, and Welding* (Ed. H.G. Suzuki) (New York: Dynamic Systems, Inc. Poestenkill: 1997), p. 395–405.
11. S.L. Semiatin and D.R. Douglas, *Rapid Heat Treatment of Nonferrous Metals and Alloys to Obtain Graded Microstructures* (US Patent 5447580: 1995).
12. O.M. Ivasishin and R.V. Teliovich, *Mater. Sci. Eng. A*, **263**, No. 2: 142–154 (1999);
https://doi.org/10.1016/S0921-5093(98)01173-3
13. P.E. Markovsky and S.L. Semiatin, *J. Mater. Process. Technol.*, **210**, No. 3: 518–528 (2010);
https://doi.org/10.1016/j.jmatprotec.2009.10.015
14. P.E. Markovsky and S.L. Semiatin, *Mater. Sci. Eng. A*, **528**, Nos. 7–8: 3079–3089 (2011);
https://doi.org/10.1016/j.msea.2010.12.002
15. V.M. Fedirko, I.M. Pogreliuk, O.I. Yaskiv, *Thermal Diffusion Multicomponent Saturation of Titanium Alloys* (Kyiv: Naukova Dumka: 2008).
16. A. Zhecheva, S. Malinov, and W. Sha, *Surf. Coat. Technol.*, **201**, No. 6: 2467–2474 (2006);
https://doi.org/10.1016/j.surfcoat.2006.04.019
17. M.Y.P. Costa, M.L.R. Venditti, M.O.H. Cioffi, H.J.C. Voorwald, V.A. Guimarres, and R. Ruas, *Int. J. Fatigue*, **33**, No. 6: 759–765 (2011);
https://doi.org/10.1016/j.ijfatigue.2010.11.007
18. H.-J. Song, M.-K. Kim, G.-C. Jung, M.-S. Vang and Y.-J. Park, *Surf. Coat. Technol.*, **201**, No. 21: 8738–8745 (2007);
https://doi.org/10.1016/j.surfcoat.2006.11.022
19. O.M. Ivasishin, P.E. Markovsky, and E.I. Sharipov, *Int. J. Mater. Prod. Technol.*, **8**, Nos. 2–4: 204–212 (1993);
https://doi.org/10.1504/ijmpt.1993.036531
20. S.V. Prikhodko, O.M. Ivasishin, P.E. Markovsky, D.G. Savvakin, and O.O. Stasiuk, *MATEC Web Conf.*, **321**: 11028 (2020);
https://doi.org/10.1051/matecconf/202032111028
21. O.M. Ivasishin, D.V. Kovalchuk, P.E. Markovsky, D.G. Savvakin, O.O. Stasiuk, V.I. Bondarchuk, D.V. Oryshych, S.G. Sedov, and V.A. Golub, *Prog. Phys. Met.*, **24**, No. 1: 75–105 (2023);
https://doi.org/10.15407/ufm.24.01.075

22. Y. Guo, P. Chen, A. Arab, Q. Zhou, and Y. Mahmood, *Def. Technol.*, **16**, No. 3: 678–688 (2020);
https://doi.org/10.1016/j.dt.2019.10.002
23. J.S. Montgomery, M.G.H. Wells, B. Roopchand, and J.W. Ogilvy, *JOM*, **49**, No. 5: 45–47 (1997);
https://doi.org/10.1007/bf02914684
24. J.S. Montgomery and M.G.H. Wells, *JOM*, **53**, No. 4: 29–32 (2001);
https://doi.org/10.1007/s11837-001-0144-2
25. S.V. Akhonin, R.N. Mishchenko, and I.K. Petrichenko, *Mater. Sci.*, **42**, No. 3: 323–329 (2006);
https://doi.org/10.1007/s11003-006-0086-5
26. O.M. Ivasishin, S.V. Akhonin, D.G. Savvakin, V.A. Berezos, V.I. Bondarchuk, O.O. Stasyuk, and P.E. Markovsky, *Prog. Phys. Met.*, **19**, No. 3: 309–336 (2018);
https://doi.org/10.15407/ufm.19.03.309
27. P.E. Markovsky, S.V. Akhonin, V.A. Berezos, V.I. Bondarchuk, O.O. Stasuk, O.P. Karasevska and I.M. Gavrysh, *Metallogr., Microstruct., Anal.*, 9(6): 856–872 (2020);
https://doi.org/10.1007/s13632-020-00705-7
28. V.M. Nesterenkov, M.O. Rusynyk, O.M. Berdnikova, V.A. Matviychuk, and R.V. Strashko, *Avtom. Svarka*, **5**: 31–36 (2020);
https://doi.org/10.37434/as2020.05.05
29. S. Akhonin, V. Nesterenkov, V. Pashynskyi, V. Matviichuk, S. Motrunich, V. Berezos, and I. Klochkov, *Eastern-European J. Enterp. Technol.*, **3**, No. 12 (129): 36–45 (2024);
https://doi.org/10.15587/1729-4061.2024.306613
30. A.N. Kalinyuk, N.P. Trigub, V.N. Zamkov, O.M. Ivasishin, P.E. Markovsky, R.V. Teliovich, and S.L. Semiatin, *Mater. Sci. Eng. A*, **346**, Nos. 1–2: 178–188 (2003);
https://doi.org/10.1016/s0921-5093(02)00518-x
31. P.E. Markovsky, D.V. Kovalchuk, J. Janiszewski, B. Fikus, D.G. Savvakin, O.O. Stasiuk, D.V. Oryshych, M.A. Skoryk, V.I. Nevmerzhytskyi, V.I. Bondarchuk, *Prog. Phys. Met.*, **24**, No. 4: 741–763 (2023);
https://doi.org/10.15407/ufm.24.04.741
32. P.E. Markovsky, J. Janiszewski, S.V. Akhonin, V.I. Bondarchuk, V.O. Berezos, K. Cieplak, O.P. Karasevska, and M.A. Skoryk, *Prog. Phys. Met.*, **23**, No. 3: 438–475 (2022);
https://doi.org/10.15407/ufm.23.03.438
33. S. Akhonin, O. Pikulin, V. Berezos, A. Severyn, O. Erokhin, and V. Kryzhanovsky, *Eastern-European J. Enterp. Technol.*, **5**, No. 12 (119): 6–12 (2022);
https://doi.org/10.15587/1729-4061.2022.265014
34. S.V. Akhonin, N.P. Trigub, V.N. Zamkov, and S.L. Semiatin, *Metall. Mater. Trans. B*, **34**, No. 4: 447–454 (2003);
https://doi.org/10.1007/s11663-003-0071-4
35. P.E. Markovsky, *Mater. Sci. Forum*, **941**: 839–844 (2018);
https://doi.org/10.4028/www.scientific.net/msf.941.839
36. A.V.K. Suryanarayana, *Testing of Metallic Materials* (Bsp Books Pvt. Limited: 2018).
37. M. Colangeli, A. De Masi, and E. Presutti, *J. Phys. A*, **50**, No. 43: 435002 (2017);
https://doi.org/10.1088/1751-8121/aa8c68
38. J. Alvarez-Ramirez, L. Dagdug, and M. Meraz, *Phys. A*, **395**: 193–199 (2014);
https://doi.org/10.1016/j.physa.2013.10.027
39. O.P. Karasevskaya, O.M. Ivasishin, S.L. Semiatin, and Y.V. Matviychuk, *Mater. Sci. Eng.*, **354**, Nos. 1–2: 121–132 (2003);
https://doi.org/10.1016/s0921-5093(02)00935-8

40. O.M. Ivasishin, P.E. Markovsky, Y.V. Matviychuk, and S.L. Semiatin, *Metall. Mater. Trans. A*, **34**, No. 1: 147–158 (2003); https://doi.org/10.1007/s11661-003-0216-8
41. O.M. Ivasishin, P.E. Markovsky, S.L. Semiatin, and C.H. Ward, *Mater. Sci. Eng. A*, **405**, Nos. 1–2: 296–305 (2005); https://doi.org/10.1016/j.msea.2005.06.027
42. G. Lütjering, *Mater. Sci. Eng. A*, **243**, Nos. 1–2: 32–45 (1998); https://doi.org/10.1016/s0921-5093(97)00778-8
43. *Titanium Alloy Ti5553* (Aubert & Duval: 2024); https://www.aubertduval.com/wp-media/uploads/sites/2/2017/06/Ti5553_GB.pdf
44. A. Caballero, A.E. Davis, J.R. Kennedy, J. Fellowes, A. Garner, S. Williams, and P. Prangnell, *Philos. Mag.*, **102**, No. 22: 2256–2281 (2022); https://doi.org/10.1080/14786435.2022.2113470
45. Y. Guo, P. Genelot, A.P. Singh, L. Bolzoni, Y. Qu, H. Kou, J. Lin, and F. Yang, *J. Mater. Eng. Perform.*, **31**: 8619–8629 (2022); https://doi.org/10.1007/s11665-022-06846-w
46. O.M. Ivasishin, P.E. Markovsky, G.A. Pakharenko, and A.V. Shevchenko, *Mater. Sci. Eng.*, **196**, Nos. 1–2: 65–70 (1995); https://doi.org/10.1016/0921-5093(94)09707-0
47. S. Suresh, *Fatigue of Materials. 2nd Edition* (Cambridge University Press: 2012); https://doi.org/10.1017/CBO9780511806575
48. W. Zhang, P. Yang, Y. Cao, X. Li, D. Wei, H. Kato, and Z. Wu, *Mater. Sci. Eng. A*, **822**: 141702 (2021); https://doi.org/10.1016/j.msea.2021.141702
49. Z. Zhong, B. Zhang, Y. Jin, H. Zhang, Y. Wang, J. Ye, Q. Liu, Z. Hou, Z. Zhang, and F. Ye, *Ceram. Int.*, **46**, No. 18: 28244–28249 (2020); https://doi.org/10.1016/j.ceramint.2020.07.325
50. P. Markovsky, J. Janiszewski, D. Savvakin, O. Stasyuk, B. Fikus, V. Samarov, V. Ellison, and S. Prikhodko, *Def. Technol.*, **39**: 1–14 (2024); https://doi.org/10.1016/j.dt.2024.04.002
51. W.J. Bruchey, *Suppression of Material Failure Modes in Titanium Armors* (Army Research Laboratory Report ARL-TR-3124: 2003).
52. J. Pu, T. Chen, Y. Sun, W. Long, H. Sun, and Y. Chen, *Coatings*, **14**, No. 9: 1096 (2024); https://doi.org/10.3390/coatings14091096
53. A. Patnaik, N. Poondla, U. Bathini, *Proc. Int. Symp. 'Processing and Fabrication of Advanced Materials — XVIII' (December 12–14, 2009, Sendai, Japan)*, vol. **2**, p. 831–848.
54. K.B. Panda and K.S. Ravi Chandran, *Metall. Mater. Trans. A*, **34**, No. 9: 1993–2003 (2003); https://doi.org/10.1007/s11661-003-0164-3
55. M. Radhakrishnan, M. Hassan, B. Long, D. Otazu, T. Lienert, and O. Anderoglu, *Additive Manufacturing*, **46**: 102198 (2021); https://doi.org/10.1016/j.addma.2021.102198
56. A. Jimoh, I. Sigalas, and M. Hermann, *Mater. Sci. Appl.*, **3**, No. 1: 30–35 (2012); https://doi.org/10.4236/msa.2012.31005
57. M. Motyka, S. Mryz, W. Więckowski, A. Stefanik, W. Ziaja, M. Poręba, and J. Adamus, *Arch. Civ. Mech. Eng.*, **24**, No. 3: (2024); https://doi.org/10.1007/s43452-024-01005-5

58. P.E. Markovsky, D.V. Kovalchuk, S.V. Akhonin, D.G. Savvakin, O.O. Stasiuk, D. Shwab, D.V. Oryshych, M.A. Skoryk, and V.P. Tkachuk, *Prog. Phys. Met.*, **24**, No. 4: 715–740 (2023);
https://doi.org/10.15407/ufm.24.04.715

Received 31.10.2024
Final version 11.11.2024

П.Є. Марковський[1], *С.В. Ахонін*[2], *В.О. Березос*[2], *О.О. Стасюк*[1], *В.І. Бондарчук*[1], *Д.В. Оришич*[1], *Є.І. Ліпчанчук*[2], *О.В. Зацарна*[1]

[1] Інститут металофізики ім. Г.В. Курдюмова НАН України, бульв. Академіка Вернадського, 36, 03142 Київ, Україна
[2] Інститут електрозварювання ім. Є.О. Патона НАН України, вул. Казимира Малевича, 11, 03150 Київ, Україна

ШАРУВАТІ МАТЕРІАЛИ НА ОСНОВІ ТИТАНУ, ВИГОТОВЛЕНІ ЛИТТЯМ І КУВАННЯМ: ВИРОБНИЦТВО, СКЛАД, МІКРОСТРУКТУРА ТА МЕХАНІЧНІ ВЛАСТИВОСТІ

Розглянуто особливості формування структури, складу й окремих механічних властивостей шаруватих матеріалів на основі титану та його сплавів, виготовлених методом електронно-променевого плавлення з проміжною ємністю. З'ясовано вплив складу окремих шарів на формування двошарових структур матеріалів: Ti64 (Ti–6Al–4V)/LCB (низьковартісного бета-Ti–1.5Al–6.8Mo–4.5Fe) і Ti64/Ti5553 (Ti–5Al–5V–5Mo–3Cr), а також 4-шарового Ti5553/Ti64/c.p.Ti (титану технічної чистоти)/Ti64. Досліджено процеси утворення перехідних прошарків між окремими сплавами як після плавлення та подальшого деформування вальцюванням, так і після термооброблень. Встановлено зв'язок між складом і сформованою мікроструктурою, з одного боку, та твердістю, міцністю, пластичністю й руйнуванням за випробувань 3-точковим вигином, з іншого боку. Проведено порівняння титанових шаруватих матеріалів, одержаних цим способом, з виготовленими із застосуванням інших технологічних підходів, а також показано переваги запропонованої технології.

Ключові слова: титанові сплави, шаруваті металеві матеріали, плавлення електронним променем з проміжною ємністю, твердість, міцність, пластичність.